Advanced Composite Materials
Publication details, including instructions for authors and subscription information:
http://www.tandfonline.com/loi/tacm20

Microscopic fatigue failure process in interleaved and toughness-improved CFRP cross-ply laminates

Nobuo Takeda [a], Shinji Ogihara [b], Akira Kobayashi [c] & Dong-Yeul Song [d]

[a] Center for Collaborative Research, The University of Tokyo, 4-6-1 Komaba, Meguro-ku, Tokyo 153, Japan

[b] Department of Mechanical Engineering, Faculty of Science and Technology, Science University of Tokyo, 2641 Yamasaki, Noda, Chiba 278, Japan

[c] Department of Mechanical Engineering, Faculty of Science and Technology, Science University of Tokyo, 2641 Yamasaki, Noda, Chiba 278, Japan

[d] Japan Fine Ceramic Center, 2-4-1 Mutsuno, Atsuta-ku, Nagoya 456, Japan

Version of record first published: 02 Apr 2012.

To cite this article: Nobuo Takeda , Shinji Ogihara , Akira Kobayashi & Dong-Yeul Song (1997): Microscopic fatigue failure process in interleaved and toughness-improved CFRP cross-ply laminates, Advanced Composite Materials, 6:4, 309-326

To link to this article: http://dx.doi.org/10.1163/156855197X00166

Adv. Composite Mater., Vol. 6, No. 4, pp. 309–326 (1997)

Microscopic fatigue failure process in interleaved and toughness-improved CFRP cross-ply laminates

NOBUO TAKEDA,[1] SHINJI OGIHARA,[2,*] AKIRA KOBAYASHI[2] and DONG-YEUL SONG[3]

[1]*Center for Collaborative Research, The University of Tokyo, 4-6-1 Komaba, Meguro-ku, Tokyo 153, Japan*
[2]*Departament of Mechanical Engineering, Faculty of Science and Technology, Science University of Tokyo, 2641 Yamasaki, Noda, Chiba 278, Japan*
[3]*Japan Fine Ceramic Center, 2-4-1 Mutsuno, Atsuta-ku, Nagoya 456, Japan*

Received 19 July 1996; accepted 13 December 1996

Abstract—Microscopic damage progress in CFRP cross-ply laminates under tensile fatigue loading was measured by the replica technique. Material systems were interleaved CFRP, T800H/3631–FM300 and toughness-improved CFRP, T800H/3900–2, with selectively toughened interlaminar layers. The damage parameter, the transverse crack density, was presented. A Paris law model was proposed, which related the cyclic strain range and the number of cycles at the transverse crack initiation. Based on the experimental data, a variational stress analysis combined with the modified Paris law was conducted to model the transverse crack multiplication.

Keywords: Fatigue; cross-ply laminates; transverse crack; microscopic damage; interleaved CFRP; toughened CFRP.

1. INTRODUCTION

The failure process of advanced composite laminates under static and fatigue loading is known to involve a sequential accumulation of damage in the form of matrix-dominated cracking. One type of damage consists of multiple transverse cracks running parallel to fibers in off-axis plies. A second type of damage consists of interlaminar delamination.

Especially in the case of CFRP laminates, due to their low interlaminar fracture toughness, delamination is the most predominant and life-limiting failure mechanism in these materials.

*To whom correspondence should be addressed.

Most methods of improving interlaminar fracture toughness are to toughen the matrix material. The increase in post-impact compressive strength and delamination toughness of composites made with tough resins have, however, been unsatisfactory.

One of relatively recent methods of toughening laminates is 'interleaving': sandwiching thin layers of resin 'interleaves' between the plies [1–7]. The interleaf approach employs two distinct resins: the matrix resin in the pre-preg sheets and the interleaf resin that provides interlaminar toughening. The major reasons for the improved delamination resistance are that the interleaf resin provides enhanced interlaminar fracture toughness and reduces the local stress concentration around the crack tip.

Another approach is to utilize the good processability of thermoset resin and high fracture toughness of thermoplastic resin [8, 9]. Hybridization of thermoset and thermoplastic resin is achieved by dispersing particulate thermoplastic polymer into thermoset base resin. The particle-dispersed layer is placed on the surface of the prepreg as a thin resin film. Hence, the heterogeneous interlaminar resin layer is formed and the interlayer fracture toughness, which directly corresponds to compressive strength after impact, is improved. An example of this approach is Torayca T800H/3900–2, developed by Toray Inc. [8, 9].

As reviewed above, investigations of the enhancement of interlaminar fracture toughness or impact resistance of interleaved or hybridized laminates have been conducted extensively. However, only a few studies of the failure process of these laminates have been conducted [10, 11].

Most of previous studies on fatigue behavior of composites involve measurements of fatigue life and stiffness reduction during fatigue loading [12, 13]. However, only a few observations of microscopic fatigue failure process have been conducted [14–19], which is necessary to identify the endurance of high performance composites.

Talreja [12, 13] proposed fatigue-life diagrams for systematic understanding of fatigue performance of composites. The fatigue-life diagram shows the number of cycles at which a certain damage mode occurs under a certain cyclic strain. Fatigue-life diagrams for on- and off-axis fatigue of unidirectional composites, for cross-ply laminates and for quasi-isotropic laminates were established. A fatigue ratio was also proposed, which was defined as the ratio of the fatigue limit to the static fracture stain. Fatigue ratio was considered to be a useful index for rating fatigue properties of composites.

Masters and Reifsnider [14] investigated the cumulative damage development in quasi-isotropic $(0/+45/-45/90)_s$ and $(0/90/+45/-45)_s$ graphite/epoxy laminates. Damage development in the form of transverse cracking in all off-axis laminae, longitudinal cracking and delamination were monitored. They found that saturated crack patterns observed were unique for each lamina in the laminate (characteristic damage state, CDS).

Wang *et al.* [15, 16] conducted a laminate failure analysis based on fracture mechanics. The simulations of transverse crack multiplication [15] and delamination growth [16] were compared with experimental results. Damage progress was well simulated with the combination of the calculation of energy release rate by finite element stress analysis and the proper estimation of critical energy release rate.

Charewicz and Daniel [17] studied damage accumulation and associated stiffness and strength reduction in cross-ply graphite/epoxy laminates under cyclic tensile loading. Stress-life data were fitted by straight lines on a log–log scale. The slope of the $S-N$ curve decreases with the number of contiguous 90° plies. Variations of residual modulus and residual strength were measured as a function of the cyclic stress level and the number of cycles.

Nairn *et al.* [18, 19] conducted fatigue experiments on several types of layups of CFRP to obtain the relation between the transverse crack density growth rate and the energy release rate range. The energy release rate was calculated by a variational stress analysis [18]. A modified Paris law was used to interpret the experimental data. It was found that the data from all layups of a single material system were found to fall on a single master Paris law plot.

In the present study, damage progress was measured by the replica technique for interleaved and toughness-improved CFRP cross-ply laminates under tensile fatigue loading. The damage parameter, transverse crack density, was presented. A Paris law model was proposed, which related the cyclic strain range to the number of cycles at transverse crack initiation. Based on the experimental data, a variational stress analysis combined with the modified Paris law was conducted to model transverse crack multiplication.

2. EXPERIMENTAL AND THEORETICAL BACKGROUND

2.1. Materials

Two material systems were used. One was interleaved CFRP, T800H/3631–FM300, with epoxy resin (FM300) layers about 100 μm thick between 0° and 90° plies. Another was toughness-improved CFRP, T800H/3900–2, with selectively toughened interlaminar layers about 30 μm thick at all the ply interfaces. The interlaminar layers have tough and fine polyamide particles dispersed in the base epoxy resin.

Constituent materials properties are shown in Table 1. T800H is a high strength carbon fiber. The 3631 is a modified epoxy system with improved toughness compared with a conventional TGDDM/DDS epoxy system. The average thickness of each ply was 0.135 mm for T800H/3631–FM300 and 0.190 mm for T800H/3900–2. The fiber volume fraction was 43.0–46.9% for T800/3631–FM300 and 54.4–54.8% for

Table 1.
Constituent material properties

	Tensile strength (MPa)	Young's modulus (GPa)	Ultimate strain (%)
Fiber			
T800H	5600	290	1.9
Resin			
3631	90.0	3.3	4.7
FM300	—	2.48	—

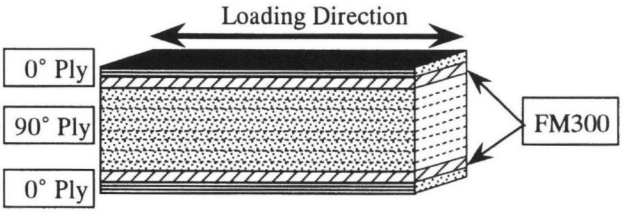

(a)

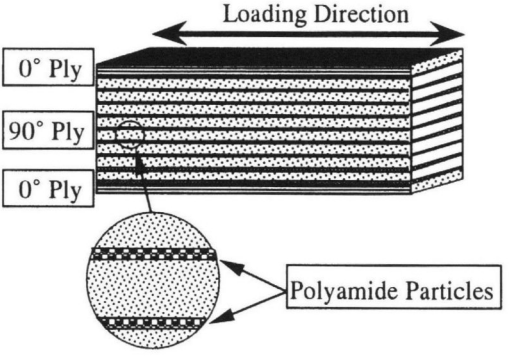

(b)

Figure 1. Schematic illustrations of the laminates used for the experiments. (a) T800H/3631–FM300 and (b) T800H/3900–2.

Table 2.
Static mechanical properties of the laminates used for the experiments

Laminates	Young's modulus (GPa)	Tensile strength (MPa)	Ultimate strain (%)
T800H/3631–FM300			
$(0/A/90_4/A/0)$	41.9	**713**	**1.70**
$(0/A/90_8/A/0)$	29.7	**456**	**1.55**
$(0/A/90_{12}/A/0)$	25.8	**373**	**1.45**
T800H/3900–2			
$(0/90_4/0)$	51.3	**970**	1.80
$(0/90_8/0)$	33.8	**543**	1.69
$(0/90_{12}/0)$	28.8	407	1.41

T800H/3900–2. The low fiber volume fraction for T800H/3631–FM300 is due to the insert of the FM300 resin film. Figure 1 shows schematic illustrations of the laminates used for the experiments.

Three different cross-ply stacking sequences (90° ply thicknesses) were prepared for both material systems. That is, $(0/A/90_m/A/0)$ (A: FM300 layer) where $m = 4$, 8 and 12, were used for T800H/3631–FM300 and $(0/90_m/0)$ where $m = 4$, 8 and

12, were used for T800H/3900–2, supplied by Toray Inc. Table 2 shows static mechanical properties of the laminates used for the experiments.

The specimen size was 100 mm long, 3 mm wide. The same specimen size was chosen as that used in our previous work [20–23] in which *in situ* observation of microscopic failure process in GFRP cross-ply laminates was conducted. GFRP tabs were glued on the specimens, which resulted in a specimen gage length of 30 mm. All specimens were stored in a desiccator to make the tests under a 'dry' condition with the water content less than 1 wt%.

2.2. *Fatigue tests*

Tensile fatigue tests were conducted at room temperature with a sine waveform under load control conditions by using an electro-hydraulic testing machine. All tests were run at the stress ratio, $R \approx 0$ and at a frequency of 5 Hz. The maximum stress levels were selected as 95%, 80%, 60%, 50% and 40% of the static tensile strength of each laminate ($s = \sigma_{max}/\sigma_B = 0.95$, 0.80, 0.60, 0.50 and 0.40, where σ_{max} is the maximum cyclic stress and σ_B is the static tensile strength of the laminate). During the fatigue tests, the testing machine was periodically stopped and the polished edge surface of a specimen was replicated on a replica film (acetyl cellulose film) with methyl acetate as resolvent. The advantages of this technique are:

(1) the damage state of a large area at each number of stress cycles can be preserved after the tests,

(2) the testing machine is stopped for only a short period, and

(3) the misalignment introduced by removing the specimen from the machine can be prevented.

The replica film was observed by optical microscopy. The number of transverse cracks in the specimen was counted to obtain the transverse crack density which was defined as the number of the transverse cracks per unit specimen length. In the present study, the fatigue damage evolution up to 10^6 cycles was observed.

2.3. *Variational stress analysis* [18]

Nairn [18] has extended Hashin's variational stress [24] analysis for cracked cross-ply laminates to include the thermal residual stresses and derived the energy release rate associated with transverse crack formation. The expression for the energy release rate, G_t, using the nomenclatures in the present study is

$$G_t = E_2^2\left(\varepsilon_0 + \varepsilon_2^T\right)^2 C_3 d Y(\rho) \quad \left(\text{for } \frac{4q}{p^2} > 1\right), \tag{1}$$

$$C_1 = \frac{(b+d)E_0}{bE_1E_2}, \qquad C_2 = \frac{\nu_{23}}{E_2}\left(\lambda + \frac{2}{3}\right) - \frac{\lambda\nu_{12}}{3E_1}, \tag{2}$$

$$C_3 = \frac{\lambda+1}{60E_2}\left(3\lambda^2+12\lambda+8\right), \qquad C_4 = \frac{1}{3}\left(\frac{1}{G_{23}}+\frac{\lambda}{G_{12}}\right),$$

$$Y(\rho) = 2\chi(\rho/2) - \chi(\rho), \tag{3}$$

$$\chi(\rho) = 2\alpha\beta\left(\alpha^2+\beta^2\right)\frac{\cosh 2\alpha\rho - \cos 2\beta\rho}{\beta\sinh 2\alpha\rho + \alpha\sin 2\beta\rho}, \tag{4}$$

$$\alpha = \frac{1}{2}\sqrt{2\sqrt{q}-p}, \qquad \beta = \frac{1}{2}\sqrt{2\sqrt{q}+p}, \tag{5}$$

$$p = \frac{(C_2 - C_4)}{C_3}, \qquad q = \frac{C_1}{C_3}, \qquad \lambda = \frac{b}{d}, \tag{6}$$

$$\rho = \frac{L}{d}, \qquad \varepsilon_2^T = -\frac{bE_1\left(\alpha_2-\alpha_1\right)}{bE_1+dE_2}\Delta T. \tag{7}$$

E_0 is laminate modulus, E_1 and E_2 are Young's moduli of 0° and 90° plies, respectively. L is the half spacing between the existing transverse cracks. G_{12} and G_{23} are axial and transverse shear moduli, respectively and ν_{12} and ν_{23} are axial and transverse Poisson's ratios, respectively. b is 0° ply thickness and d is half thickness of 90° ply. ε_2^T thermal residual strain in 90° ply. α_1 and α_2 are axial and transverse thermal expansion coefficient, respectively. ΔT is the difference between testing and curing temperatures.

2.4. *Modified Paris law model* [18, 19]

The conventional Paris law approach relates the crack growth rate to the range in the applied stress intensity factor. Nairn *et al.* [18, 19] proposed analyzing fatigue data using a modified Paris law approach. In their analysis, the energy release rate range was used instead of the range in stress intensity factor and the transverse crack density was substituted instead of the crack length. The energy release rate was calculated by the variational stress analysis.

They found that the data from all layups of a single material system fell on a single master Paris law plot. The master Paris law plot was used to characterize the resistance to the transverse crack formation during fatigue loading for a given material system.

The modified Paris law equation can be written as,

$$\frac{\mathrm{d}\rho}{\mathrm{d}n} = A_t\left(\Delta G_t\right)^{\gamma_t}, \tag{8}$$

$$\Delta G_t = G_t\big|_{\sigma_0=\sigma_{\max}} - G_t\big|_{\sigma_0=\sigma_{\min}}, \tag{9}$$

where n is the number of cycles, σ_{max} and σ_{min} is the applied maximum and minimum stresses, A_t and γ_t are constants. The energy release rate range, ΔG_t, can be calculated using equation (1).

3. EXPERIMENTAL RESULTS

Figure 2 shows $S-N$ curves for (a) T800H/3631–FM300 and (b) T800H/3900–2, cross-ply laminates. Because the final fracture of the cross-ply laminates occurs when the 0° plies break, the $S-N$ curves are rather flat. In the present study, the damage progress in the laminates during fatigue loading is focused rather than the fatigue life of the laminates. In all the cross-ply laminates, the first microscopic damage observed was transverse cracks which ran through the thickness of the 90° plies.

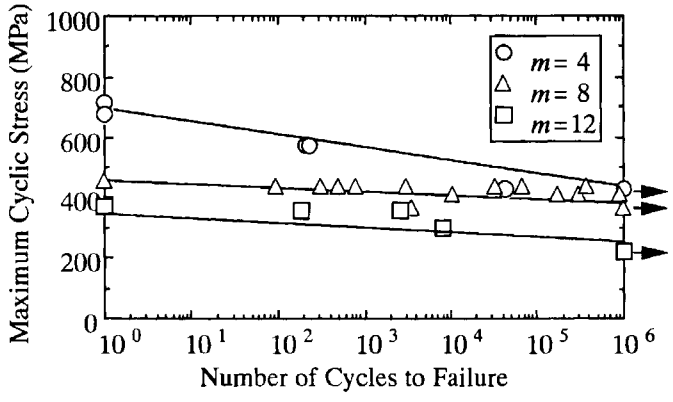

(a)

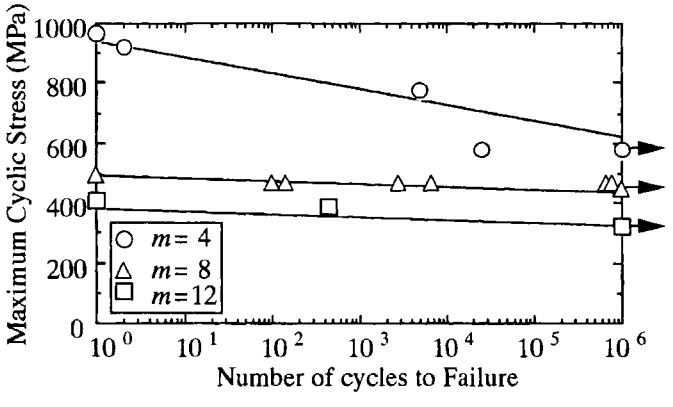

(b)

Figure 2. $S-N$ curves for (a) T800/3631–FM300 (0/A/90_m/A/0) and (b) T800/3900–2 (0/90_m/0), cross-ply laminates.

Figure 3 shows a transverse crack in T800H/3631–FM300 (0/A/90_4/A/0) at s = 0.60 ((a) n = 5000, (b) n = 100 000). Figures 3 (a) and (b) show the same transverse crack tip for different number of cycles. At transverse crack initiation, a transverse crack runs through the thickness of the 90° layer and the transverse crack tip stops at the 90°/FM300 layer interface. As the number of cycles increases, the transverse crack tip propagates into the FM300 layer as shown in Fig. 3(b).

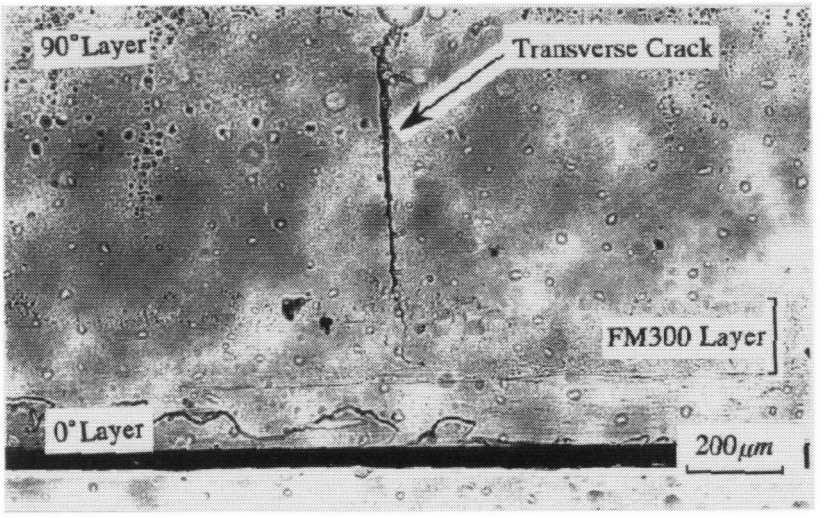

(a)

(b)

Figure 3. A transverse crack in T800H/3631–FM300 (0/A/90_4/A/0) at s = 0.60 ((a) n = 5000, (b) n = 100 000).

The number of transverse cracks increases as the number of cycles increases. Figure 4 shows transverse crack density as a function of the number of cycles. As the maximum cyclic stress increases, the transverse cracks occur in the earlier stage. However, the saturated level of the transverse crack density is similar for a laminate configuration even at different maximum cycle stresses. The saturated transverse crack density decreases at the number of 90° plies increases.

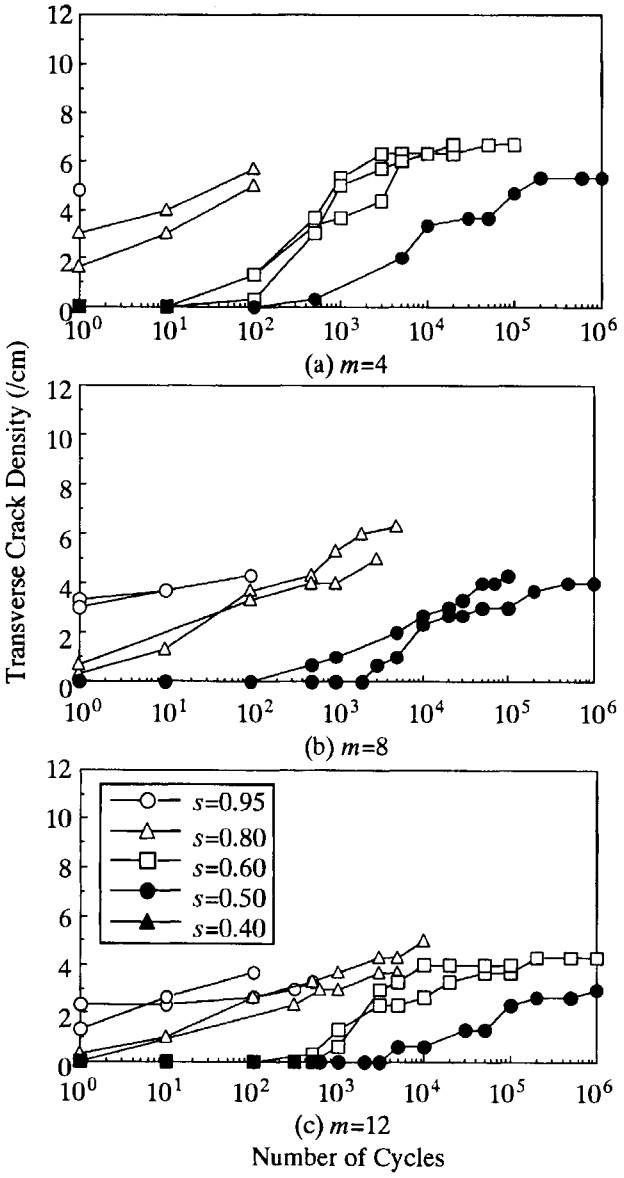

Figure 4. Transverse crack density as a function of the number of cycles for T800H/3631–FM300 cross-ply laminates.

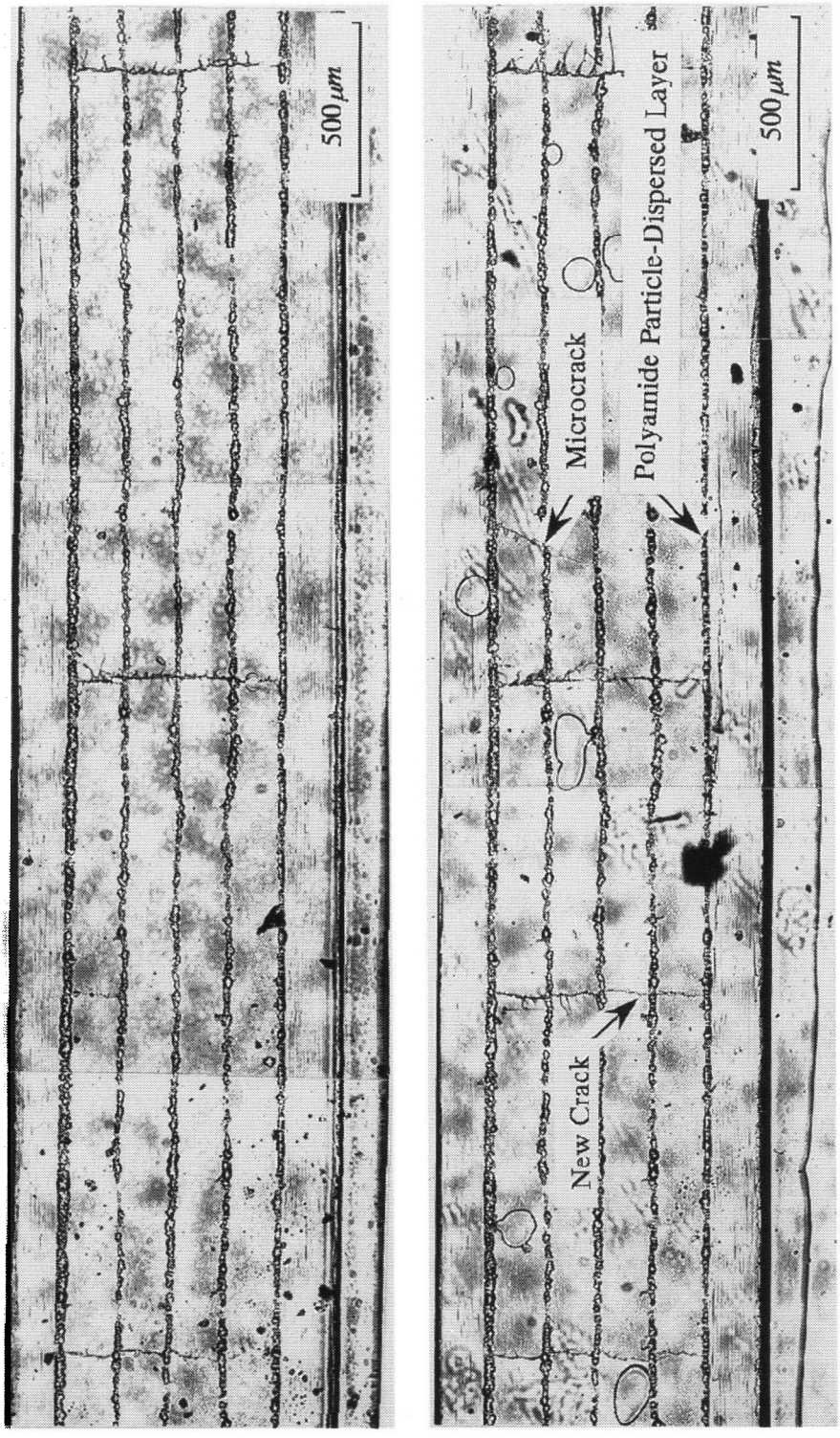

Figure 5. Transverse crack multiplication in T800H/3900–2 $(0/90_4/0)$ at $s = 0.80$ (top: $n = 1$, bottom: $n = 500$).

Figure 5 shows the transverse crack multiplication in T800H/3900–2 ($0/90_4/0$) at $s = 0.80$ (top: $n = 1$, bottom: $n = 500$). In Fig. 5(bottom), formation of a new transverse crack and a microcrack is observed. Figure 6 shows transverse crack density as a function of the number of cycles. Similar to the T800H/3631–FM300 system, the saturated level of the transverse crack density is similar for a laminate configuration at the different maximum cyclic stresses and the saturated transverse crack density decreases as the number of 90° plies increases.

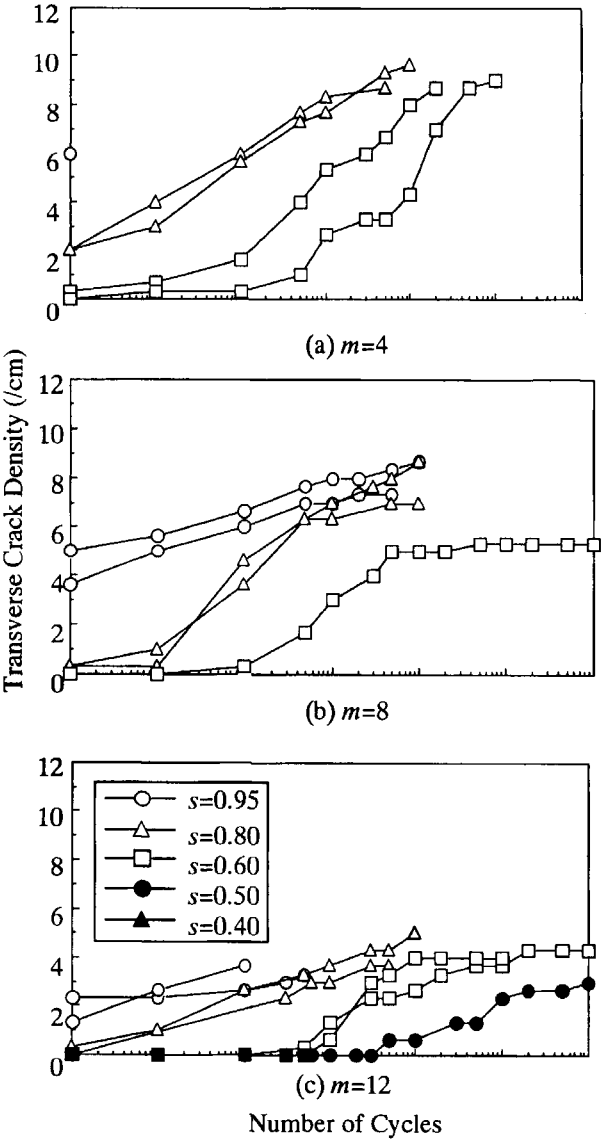

Figure 6. Transverse crack density as a function of the number of cycles for T800H/3900–2 cross-ply laminates.

4. DISCUSSION

4.1. A Paris law analysis for transverse cracking initiation

In this section, a Paris law analysis is presented to model the initiation of transverse cracks. Transverse cracks can be considered to initiate from inherent microscopic flaws. Figure 7 shows assumed transverse crack initiation mechanism. The initial flaw (length a_0) propagates in the thickness direction by the fatigue loading. When the flaw length, a, reaches the critical value, a_c unstable growth of the flaw occurs and a transverse crack is formed.

$$K_c = E_2 \varepsilon \sqrt{\pi a_c}, \tag{10}$$

where K_c is the fracture toughness of the 90° ply and ε is the maximum strain in 90° ply during fatigue loading.

Assuming that growth of the flaw obeys the Paris law, the growth rate is expressed as

$$\frac{da}{dn} = C_p(\Delta K)^{m_p}, \tag{11}$$

where C_p and m_p are constants and

$$\Delta K = E_2 \Delta\varepsilon \sqrt{\pi a}, \quad \Delta\varepsilon = (1 - R)\frac{\sigma_{max}}{E_0}. \tag{12}$$

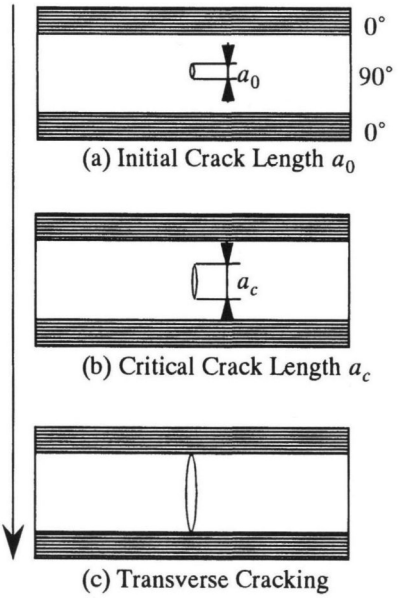

Figure 7. Assumed transverse crack initiation mechanism.

Table 3.
Parameters used for the Paris law model prediction of transverse crack initiation

Material system	a_0 (μm)	C_p	m_p
T800H/3631–FM300	4.8	0.30	12
T800H/3900–2	4.4	0.27	10

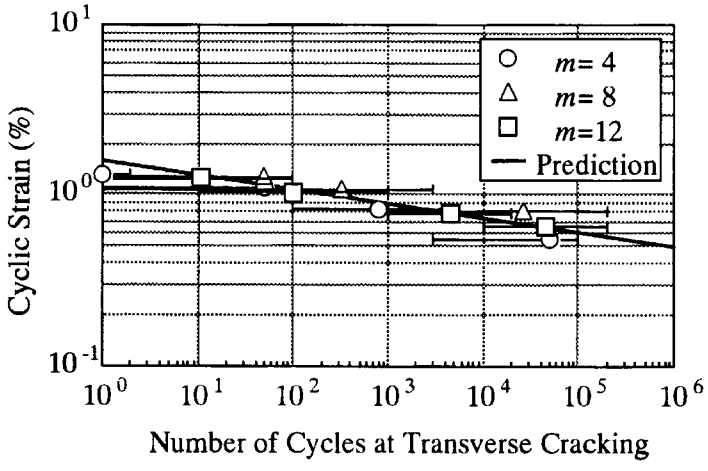

(a)

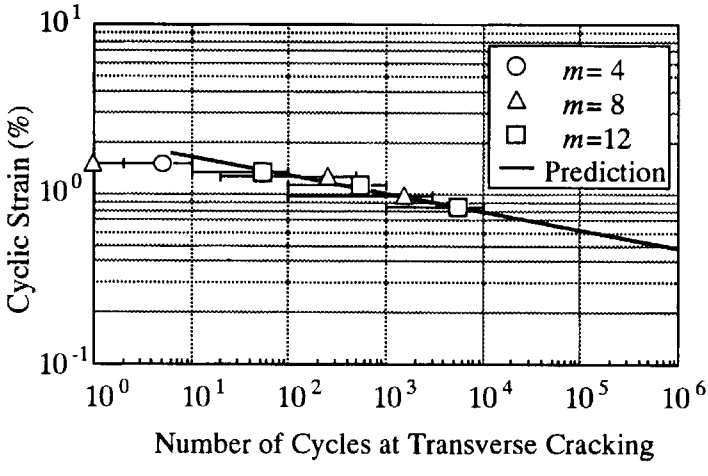

(b)

Figure 8. Comparison between the experimental results and the model prediction of the number of cycles at transverse cracking for (a) T800H/3631–FM300 and (b) T800H/3900–2 cross-ply laminates.

Substituting equation (12) into equation (11) and integrating from a_0 to a_c,

$$\int_{a_0}^{a_c} \frac{da}{m_p/a^2} = \int_0^{N_t} C_p\left(\sqrt{\pi} E_2 \Delta\varepsilon\right)^{m_p} dn, \tag{13}$$

that is,

$$\left[\left(-\frac{m_p}{2}+1\right)a^{-\frac{m_p}{2}+1}\right]_{a_0}^{a_c} = C_p\left(\sqrt{\pi} E_2 \Delta\varepsilon\right)^{m_p} N_t, \tag{13'}$$

where N_t is the number of cycles at transverse cracking. Assuming that $a_0 \ll a_c$, the value of left hand of equation (13′) when $a = a_c$ is assumed to be negligible and set to zero, then,

$$N_t = \frac{(\Delta\varepsilon)^{-m_p}}{C_p\left(\sqrt{\pi} E_2\right)^{m_p}\left(\frac{m_p}{2}-1\right)a_0^{\frac{m_p}{2}-1}}. \tag{14}$$

This equation means that the log–log plot of $\Delta\varepsilon$ and N_t falls on a straight line for a material system.

To discuss the validity of the present model, a comparison with the experimental data was conducted. Table 3 shows assumed parameters used in the present model. The initial flaw length was assumed to be the same order of the fiber diameter. The diameter of T800H carbon fiber is about 5 μm. Figure 8 shows comparison between the experimental results and the model prediction of the number of cycles at transverse cracking for (a) T800H/3631–FM300 and (b) T800H/3900–2 cross-ply laminates. As shown in the figures, the present model can fit the experimental results using the assumed parameters.

4.2. Modified Paris law analysis for transverse crack multiplication

In this section, the modified Paris law analysis for transverse cracking was conducted following Nairn [18, 19]. Material properties used for the variational analysis are shown in Table 4.

Table 4.
Material properties used for the Paris law analysis for transverse crack multiplication

	T800H/3631–FM300	T800H/3900–2
E_1 (GPa)	152.2	130.4
E_2 (GPa)	9.57	7.96
G_{12} (GPa)*	4.50	4.50
G_{23} (GPa)*	3.21	3.21
ν_{12}*	0.349	0.349
ν_{23}*	0.490	0.490
$\alpha_1(\times 10^{-6}/°C)$	0.10	−1.73
$\alpha_2(\times 10^{-6}/°C)$	35.5	34.7
ΔT(°C)	−160	−160

*Assumed value.

Figure 9 shows the transverse crack density growth rate, $d\rho/dn$, as a function of the energy release rate range, ΔG_t for (a) T800H/3631–FM300 and (b) T800H/3900–2 cross-ply laminates. In calculation of the energy release rate of T800H/3631–FM300, the FM300 layer was considered as a part of the 90° ply, that is, the total thickness of 90° ply and FM300 layer was used as the thickness of 90° ply in equation (1).

If the application of the Paris law is valid, all the data for a material system should fall on a single straight line. For both systems, the obtained lines for each laminate configuration were quite different from each other. The reason for this is considered for each material system.

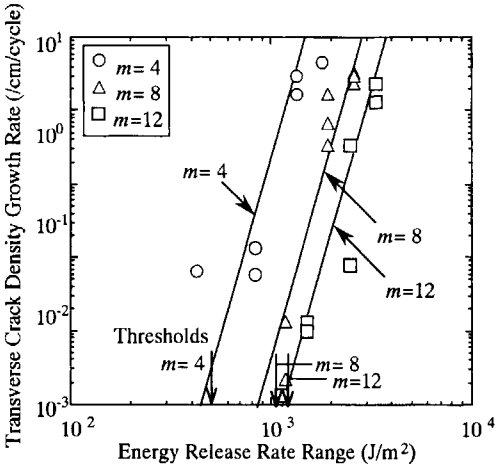

Figure 9. Transverse crack density growth rate, $d\rho/dn$, as a function of the enrgy release rate range, ΔG_t.

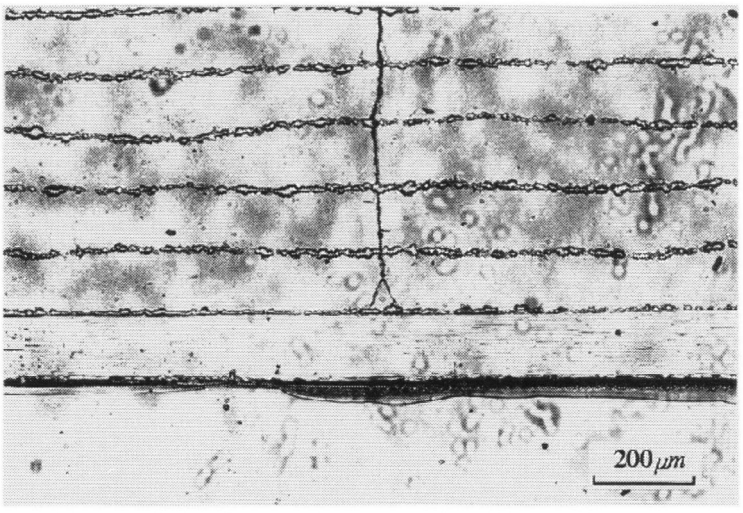

(a)

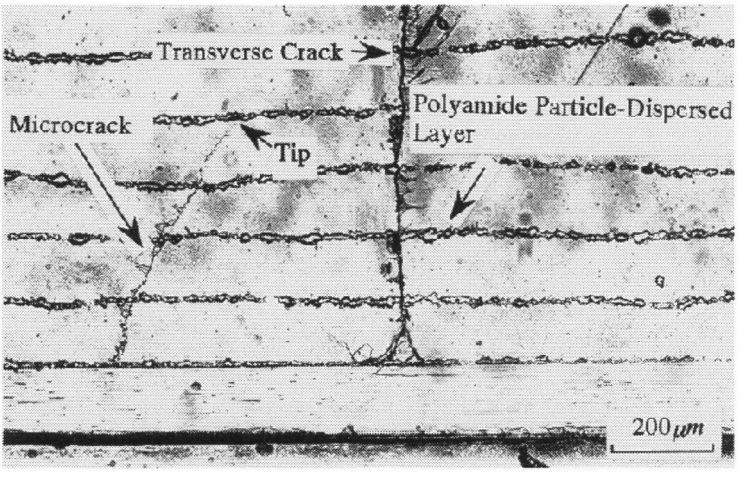

(b)

Figure 10. Microcrack formation near the transverse crack tip in T800H/3900–2 $(0/90_{12}/0)$ at $s = 0.60$ ((a) $n = 1000$, (b) $n = 5000$).

For T800H/3631–FM300, the accuracy of the calculated energy release rate may not be enough. In this study, the FM300 layer was considered as a part of the 90° ply, but the transverse cracks did not penetrate into the FM300 layer at an earlier stage, as shown in Fig. 3(a). An analysis considering the interlaminar layer is necessary.

For T800H/3900–2, the formation of microcracks around the transverse crack tip must be considered. Figure 10 shows microcrack formation near the transverse crack tip in T800H/3900–2 $(0/90_{12}/0)$ at $s = 0.60$ ((a) $n = 1000$, (b) $n = 5000$). Micro-

cracks occur at some angles from the 0°/90° interface due to a large shear deformation around the transverse crack tip. The large shear deformation is attributed to reduction in total shear modulus by inserting the polyamide particle-dispersed layers.

After microcracks occur, the stress state in the 90° ply should be changed drastically and the accuracy of the energy release rate is reduced. The microcracks often occur in the laminate with thicker 90° plies. Thus, a Paris law line obtained for the laminated with thinner 90° ply, such as $m = 4$, may represent the essential material property.

In Fig. 9, the thresholds in the figure indicate the energy release rate ranges corresponding to the maximum cyclic strains at which no transverse cracking occurred up 10^6 cycles. In general, data like this may be important for designing and ranking the fatigue resistance of composite materials.

5. CONCLUSIONS

(1) Fatigue damage progress was investigated microscopically for interleaved CFRP, T800H/3631–FM300 and toughness-improved CFRP, T800H/3900–2 cross-ply laminates. A progressive damage parameter, the transverse crack density, was measured by the replica technique.

(2) A Paris law analysis was presented to model the initiation of the transverse cracking. A model assuming that a transverse crack occurs as a result of inherent flaw growth proved to be valid to characterize the transverse crack initiation

(3) Transverse crack growth was analyzed using the modified Paris law combined with the variational stress analysis. The modified Paris law may be applicable for the laminates with thin 90° layers. However, for the laminates with thicker 90° layer, further improvement is required.

REFERENCES

1. Browning, C. E. and Schwartz, H. S. Delamination resistant composite concepts. *ASTM STP* **893**, 256–265 (1986).
2. Chan, W. S., Rogers, C. and Aker, A. Improvement of edge delamination strength of composite laminates using adhesive layers. *ASTM STP* **893**, 266–285 (1986).
3. Norman, T. L. and Sun, C. T. Mechanical properties and interlaminar toughness of cross-plied laminates containing adhesive strips. *AIAA Journal* **29**, 247–252 (1991).
4. Ozdil, F. and Carlsson, L. A. Finite element analysis of interleaved DCB specimen. *Engng Fracture Mech.* **41**, 475–485 (1992).
5. Ozdil, F. and Carlsson, L. A. Plastic zone estimates in mode I interlaminar fracture of interleaved composites. *Engng Fracture Mech.* **41**, 645–658 (1992).
6. Askoy, A. and Carlsson, L. A. Interlaminar shear fracture of interleaved graphite/epoxy composites. *Compos. Sci. Technol.* **43**, 55–69 (1992).
7. Jones, R. M. Delamination-suppression concepts for composite laminate free edges. In: *Proc. ICCM/8.* Honolulu, HI (1991), pp. 28-M-1–28-M-10.
8. Odagiri, N., Muraki, T. and Tobukuro, K. Toughness improved high performance torayca prepreg T800H/3900 series. In: *33rd International SAMPE Symposium.* Anaheim, CA (1988), pp. 272–283.
9. Odagiri, N., Kishi, H. and Nakae, T. T800H/3900-2 toughened epoxy prepreg system: toughening concept and mechanism. In: *Proc. Amer. Soc. Compos. 6th Technical Conf.* Troy, NY (1991), pp. 43–52.

10. Altus, E. and Ishai, O. Trnasverse cracking and delamination interaction in the failure process of composite laminates. *Compos. Sci. Technol.* **26**, 59–77 (1986).
11. Altus, E. and Ishai, O. The effect of soft interleaved layers on the combined transverse cracking/delamination mechanisms in composite laminates. *Compos. Sci. Technol.* **39**, 13–27 (1990).
12. Talreja, R. Fatigue of composite materials: damage mechanisms and fatigue-life diagrams. *Proc. Roy. Soc. Lond.* **A378**, 461–475 (1981).
13. Talreja, R. A conceptual framework for the interpretation of fatigue damage mechanisms in composite materials. *J. Comp. Technol. Res.* **7**, 25–29 (1985).
14. Masters, J. E. and Reifsnider, K. L. An investigation of cumulative damage development in quasi-isotropic graphite/epoxy laminates. *Damage in Composite Laminates, ASTM STP* **775**, 40–62 (1982).
15. Wang, A. S. D. Fracture mechanics of sublaminate cracks in composite materials. *Comp. Technol. Rev.* **6**, 45–62 (1984).
16. Wang, A. S. D., Slominia, M. and Bucinell, R. B. Delamination crack growth in composite laminates. *Delamination and Debonding of Materials, ASTM STP* **876**, 135–167 (1985).
17. Charewicz, A. and Daniel, I. M. Damage mechanisms and accumulation in graphite/epoxy laminates. *Composite Materials: Fatigue and Fracture, ASTM STP* **907**, 274–297 (1986).
18. Nairn, J. A. Microcracking, microcrack-induced delamination and longitudinal splitting of advanced composite structures. NASA CR4472 (1992).
19. Liu, S. and Nairn, J. A. Fracture mechanics analysis of composite microcracking: experimental results in fatigue. In: *Proc. 5th Tech. Conf. Comp. Mater.* American Society for Composites (1990), pp. 287–295.
20. Takeda, N. and Ogihara, S. *In situ* observation and probabilistic prediction of microscopic failure process in CFRP cross-ply laminates. *Compos. Sci. Technol.* **52**, 183–195 (1994).
21. Takeda, N. and Ogihara, S. Initiation and growth of delamination from the tips of transverse cracks in CFRP cross-ply laminates. *Compos. Sci. Technol.* **52**, 309–318 (1994).
22. Ogihara, S. and Takeda, N. Interaction between transverse cracks and delamination during damage progress in CFRP cross-ply laminates. *Compos. Sci. Technol.* **54**, 395–404 (1995).
23. Takeda, N., Ogihara, S. and Kobayashi, A. Microscopic fatigue damage progress in CFRP cross-ply laminates. *Composites* **26**, 859–867 (1995).
24. Hashin, Z. Analysis of cracked laminates: a variational approach. *Mechan. Mater.* **4**, 121–136 (1985).